Available online at www.sciencedirect.com
SCIENCE DIRECT®
Atmospheric Environment 39 (2005) 2545–2552
ATMOSPHERIC ENVIRONMENT
www.elsevier.com/locate/atmosenv

Investigation of urban atmospheric visibility by high-frequency extraction: Model development and field test

Chin-Hsiang Luo[a,*], Che-Yen Wen[b], Chung-Shin Yuan[c], Jiun-Jian Liaw[d], Cho-Ching Lo[c], Shih-Hsuan Chiu[d]

[a]*Department of Environmental Engineering, Hung-Kuang University, 34, Chung-Chie Road, Taichung, Taiwan, ROC*
[b]*Department of Forensic Science, National Central Police University, 56, Shu-Ren Road, Da-Gang, Guei-Shan, Tao-Yuan, Taiwan, ROC*
[c]*Institute of Environmental Engineering, National Sun Yat-Sen University 70, Lien-Hai Road, Kaohsiung, Taiwan, ROC*
[d]*Department of Polymer Engineering, National Taiwan University of Science and Technology, 43, Kee-lung Road, Section 4, Taipei, Taiwan, ROC*

Received 17 May 2004; received in revised form 11 December 2004; accepted 7 January 2005

Abstract

This work investigates atmospheric visibility by employing two statistical processes for high-frequency extraction: Sobel operator and fast Fourier transform (FFT). In replacing the traditional measurement methods for atmospheric visibility, the new approaches can provide accurate digital data urban visibility by establishing the numerical indices. The procedure is illustrated as follows. Digital images of urban areas in Kaohsiung, a city at the south of Taiwan, are analyzed according to brightness. High-frequency components of the image are extracted to calculate the index values by employing the Sobel operator and FFT. Finally, the correlation between each index and the visual range estimated by trained investigators are evaluated. A good correlation between two indices and the values obtained by visual investigation is affirmed by correlation coefficients (R^2), 0.8139 and 0.7797, respectively. Furthermore, both indices are highly correlated with each other ($R^2 = 0.9173$). Convenient transmission and the exchangeability of digital images of the real-time landscape facilitate the publication of results on the world wide web (WWW).

Keywords: Visibility; Frequency extraction; Image processing; Air quality

1. Introduction

Urban atmospheric visibility can influence the overall quality for residents in a geographic area, and the experience of tourists visiting that area. Impairment of visibility also strongly implies the presence of atmospheric pollution. Ambient pollutants, particulate matter and few gaseous species (nitrogen dioxide and ozone), markedly decrease visual range (Dzubay et al., 1982; Tsai and Cheng, 1997; Yuan and Yang, 1997; Sequeira and Lai, 1998). Atmospheric visibility has not only attracted the attention of the public, including that of those who create air-quality regulations, but also provides a useful way for investigating variations in the atmosphere (Watson, 2002).

Traditional investigations of visibility, such as those for traffic safety or aviation, focus on whether selected targets in a concerned area are visible. Visibility is scientifically defined as the maximum distance at which the outlines of selected targets can be recognized against

*Corresponding author. Tel.: +886 4 26318652; fax: +886 4 26525245.
E-mail address: andyluo@sunrise.hk.edu.tw (C.-H. Luo).

1352-2310/$ - see front matter © 2005 Elsevier Ltd. All rights reserved.
doi:10.1016/j.atmosenv.2005.01.023

a horizon background (Horvath, 1981). This distance in atmospheric investigations is the meteorological range of atmospheric environment. In such investigations, the targets, ideally, should be black. If a black target is not available, the alternative color must be sufficiently dark that it is distinguishable with background. Visibility is equal to the distance at which the farthest target can be recognized. Spacing of selected targets therefore restricts the accuracy of the traditional visibility measurements.

Some models and modified formulas (Williams et al., 1981; Babson et al., 1982; Malm and Molenar, 1984; Larson et al., 1988) for measuring visibility have applied photograph processing methods to calculate or improve various parameters related to atmospheric visibility. Such efforts have also tried to discern the influence of numerous important factors affecting visibility: size distribution and scattering properties of suspended aerosols; weather interference; chemical composition of pollutants, etc. However, complicated procedures are not adequate for describing the real-time atmospheric visibility. According to the definition of Weber's ratio (Gonzalez and Woods, 2002) and a contrast between target and background (Pitchford and Malm, 1994), Luo et al. (2002) translated digital image data for a nearly perfect target, an urban skyscraper, to values of specific brightness (the brightness difference between the skyscraper and its background). A good linear correlation between the values of specific brightness and visual measurements obtained by trained investigators was established for visual range of 5–10 km. A major advancement in the work of Luo et al. (2002) was to provide real-time measurement of visibility and characteristic images in particular areas. But the selection and appearance of an ostensibly perfect target is still a difficult problem in this approach.

Image recognition has been widely applied in recent years to astronomy, meteorology, aviation and satellite technology, biology, medical analysis, national defense technology, industrial design, geographic information system (GIS), security, environmental monitoring, etc. Image enhancement, a process for image recognition, is a novel application for measuring atmospheric visibility without the existence of a perfect target. An enhancement process can be implemented in the spatial domain (image domain) or frequency domain of visual information records, such as a two-dimensional scene image. A key method for processing image pixels (spatial domain) is to establish a mathematically generated mask (such as a filter, kernel, template or window). Conversely, the frequency domain operators work on the Fourier series data which represent the pre-transferred scene image. Furthermore, the spatial characteristics (such as scenery texture) can be presented by these enhancement methods that discriminate gray levels between any target and the image background.

This work proposes a novel technique for measuring atmospheric visibility by applying a Sobel mask and FFT (fast Fourier transform) to the urban area in Kaohsiung. Two independent indices derived by Sobel mask and FFT are used to automatically monitor the visibility. The effectiveness of this technique is evaluated.

2. Frequency extraction from an image

2.1. Digital imaging for visibility measurement

A gray level image can be presented by one component, brightness, while a color image requires three components (red, green, and blue). Brightness difference in environmental images is an important factor in measuring visibility (Middleton, 1963). A digital image acquired in the field acquisition provides the data for space dimension and gray level (digital brightness). These data are, then, mathematically translated and employed in the $M \times N$ matrix (Petrou and Bosdogianni, 1999):

$$f(x,y) = \begin{bmatrix} f(0,0) & \cdots & f(0,N-1) \\ \vdots & & \\ f(M-1,0) & \cdots & f(M-1,N-1) \end{bmatrix}. \quad (1)$$

The value in the matrix function is that it presents the gray level at any location of (x, y). Each element in the matrix is a pixel (or image element). Gray levels are 2^k and estimated by sampling hardware (i.e., digital camera). The resulting image is a k-bit image. All images for urban atmospheric visibility measurements in this study are 8-bit; their gray level values range from 0 to 255. The gray level value of 0 is set as perfect black. As such, brightness increases as the gray level value increases.

Since a color image is produced in three standard components (red, $\lambda = 700$ nm, green, $\lambda = 546$ nm, and blue, $\lambda = 436$ nm), any pixel in the color image consists of brightness values for three colors: L_R (red), L_G (green) and L_B (blue). The wavelength of a component is represented by λ. A color image is converted into a gray level image (brightness L) with

$$L = \frac{L_R + L_G + L_B}{3}. \quad (2)$$

Total L values for the sampled image were analyzed with Eq. (2), then the modified data were saved in the format shown in Eq. (1).

2.2. Model description

Visual recognition by human perception requires signal change emitted from a target. This signal is primarily the target's brightness or gray level. For image

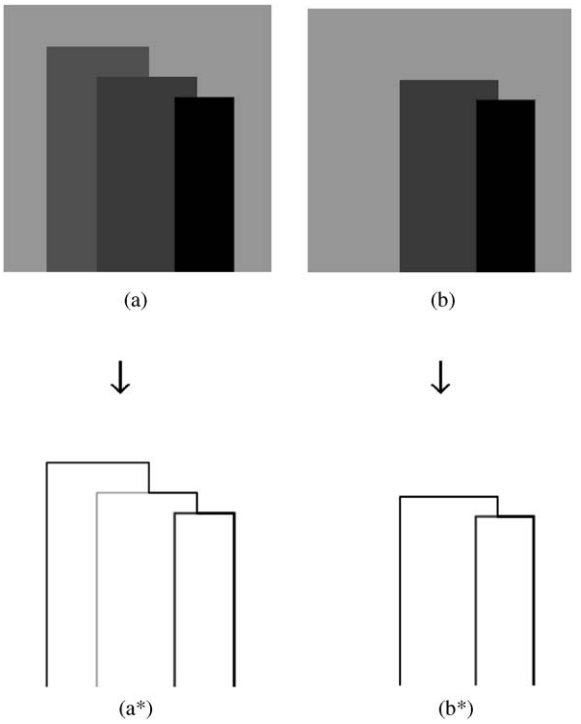

Fig. 1. Two synthetic images applied to demonstrate the high-frequency model for visibility. There is better visibility shows in (a) than (b), (a*) and (b*) are the high-frequency maps for (a) and (b), respectively.

processing, high-frequency components represent signal disturbance. Fuzzy scenes or impaired visibility produced by foggy weather or heavy haze cannot appear detailed, and high-frequency components in the scene image decrease.

Two synthetic images (Fig. 1) are used to demonstrate two visibility types. Obviously, the image in Fig. 1(a) has better visibility than the image in Fig. 1(b) because of more complicated texture and signal disturbance appearing in the Fig. 1(a) image. High-frequency components in the image in Figs. 1(a) and (b) are extracted and shown in Figs. 1(a*) and (b*), respectively. Fig. 1(a*) has more high-frequency components than Fig. 1(b*).

Sobel mask and FFT are popular extraction methods for extracting high-frequency components in images. These are briefly summarized as follows.

2.3. Sobel mask

A 3×3 mask (a mathematic matrix) is illustrated as

$$\begin{bmatrix} w_1 & w_2 & w_3 \\ w_4 & w_5 & w_6 \\ w_7 & w_8 & w_9 \end{bmatrix}$$

Response (R) of every pixel on the digital image is processed by the following equation:

$$R = w_1 z_1 + w_2 z_2 + \cdots + w_9 z_9 = \sum_{i=1}^{9} w_i z_i, \tag{3}$$

where w_i's are the weighting coefficients in the 3×3 mask and z_i's are the gray level values (digital brightness) of corresponding points in the image. Sobel masks are shown as

$$\underbrace{\begin{bmatrix} -1 & -2 & -1 \\ 0 & 0 & 0 \\ 1 & 2 & 1 \end{bmatrix}}_{G_x} \text{ or } \underbrace{\begin{bmatrix} -1 & 0 & 1 \\ -2 & 0 & 2 \\ -1 & 0 & 1 \end{bmatrix}}_{G_y},$$

i.e.,

$$Gx = (z_7 + 2z_8 + z_9) - (z_1 + 2z_2 + z_3), \tag{4}$$

$$Gy = (z_3 + 2z_6 + z_9) - (z_1 + 2z_4 + z_7). \tag{5}$$

The G value of the pixel located by the center point of the mask can be computed by

$$G = \nabla f = |Gx| + |Gy|. \tag{6}$$

The computations in Eqs. (4)–(6) are repeated pixel by pixel around the whole image. Finally, an index value for the Sobel operation is expressed by the average of G values for all points in an image. Because brightness noises improve the occurrence of high-frequency components, the Sobel operator can identify the discrepancy and gradient between any two points in the image in the spatial domain (Gonzalez and Woods, 2002).

2.4. High-pass filtering with FFT

The discrete Fourier transform (DFT) of the image of $M \times N$ dimension, $f(x, y)$, can be expressed as

$$F(u, v) = \frac{1}{MN} \sum_{x=0}^{M-1} \sum_{y=0}^{N-1} f(x, y) \times \exp[-j2\pi(ux/M + vy/N)]. \tag{7}$$

First, the image (spatial domain) with the frequency domain spectrum is presented by Eq. (7). Second, a cutoff radius (C_R, unit: pixel) is set to erase the information of low-frequency information in the spectrum. This tool is called a high-pass filter. In practice, FFT rather than DFT is typically adopted because of FFT's simplicity and saving time for computing (Gonzalez and Woods, 2002). Furthermore, the C_R value was set to 5–30 pixels in this work. The reason

for using this range of the C_R values will be discussed in Section 3.2. Finally, the filtered image can be generated by

$$f(x,y) = \sum_{u=0}^{M-1} \sum_{v=0}^{N-1} F(u,v) \exp[j2\pi(ux/M + vy/N)] \quad (8)$$

The average gray level of this projection is valued as a FFT index.

2.5. Extraction test

The two extraction processes are tested with a synthetic image shown in Fig. 2(a). In the spatial domain, the Sobel mask screens high-frequency components of the artificial image, then the gradient mapping shown in Fig. 2(b) is utilized. Next, FFT transfers the same image into the frequency domain. The low-frequency components in the frequency spectrum are cut off with a defined radius ($C_R = 30$ pixels). Fig. 2(c) presents the remaining map which is finally transferred to high-frequency pass information of, Fig. 2(d), in the spatial domain.

3. Application to urban atmospheric images

3.1. Image sampling

The location for this investigation is on the top of the Linden Hotel, a famous 42-floor landmark in the center of Kaohsiung city. The altitude of this site is 175 m above sea level. Twelve targets settled to the north of the sampling site were orientated with GPS (global positioning system). These targets include skyscrapers, dark-colored buildings, chimney stacks, and the boundary line between mountains and sky. The distances between the targets and sampling site range from 0.5 to 15 km.

Recording and transmission of image acquisition and visual observation results were processed at the same time, and schematically shown in Fig. 3. Instruments used included four specific devices: a processor for frequency extraction; controller for camera operation; web server; and a router. Two computing programs for the Sobel mask and FFT high-pass filter were installed computer's processor. For visual observations, the northern visual range (unit: km) for urban scenery was detected by the trained investigators. To decrease discrepancies among human visual measurements, all investigators participated in the training courses and

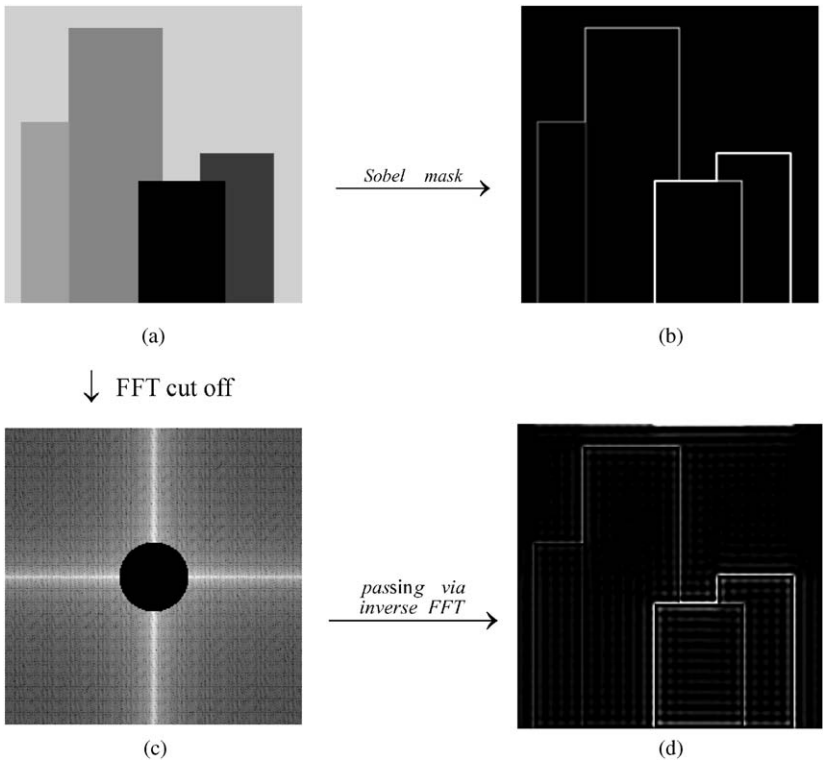

Fig. 2. The two extraction processes: Sobel mask and FFT. (a) a synthetic image; (b) the result of spatial filtering by Sobel mask; (c) the result of low-frequency cutoff (radius = 30 pixels, solid black core) artificially operated after FFT; and (d) high-frequency information pass via inverse FFT.

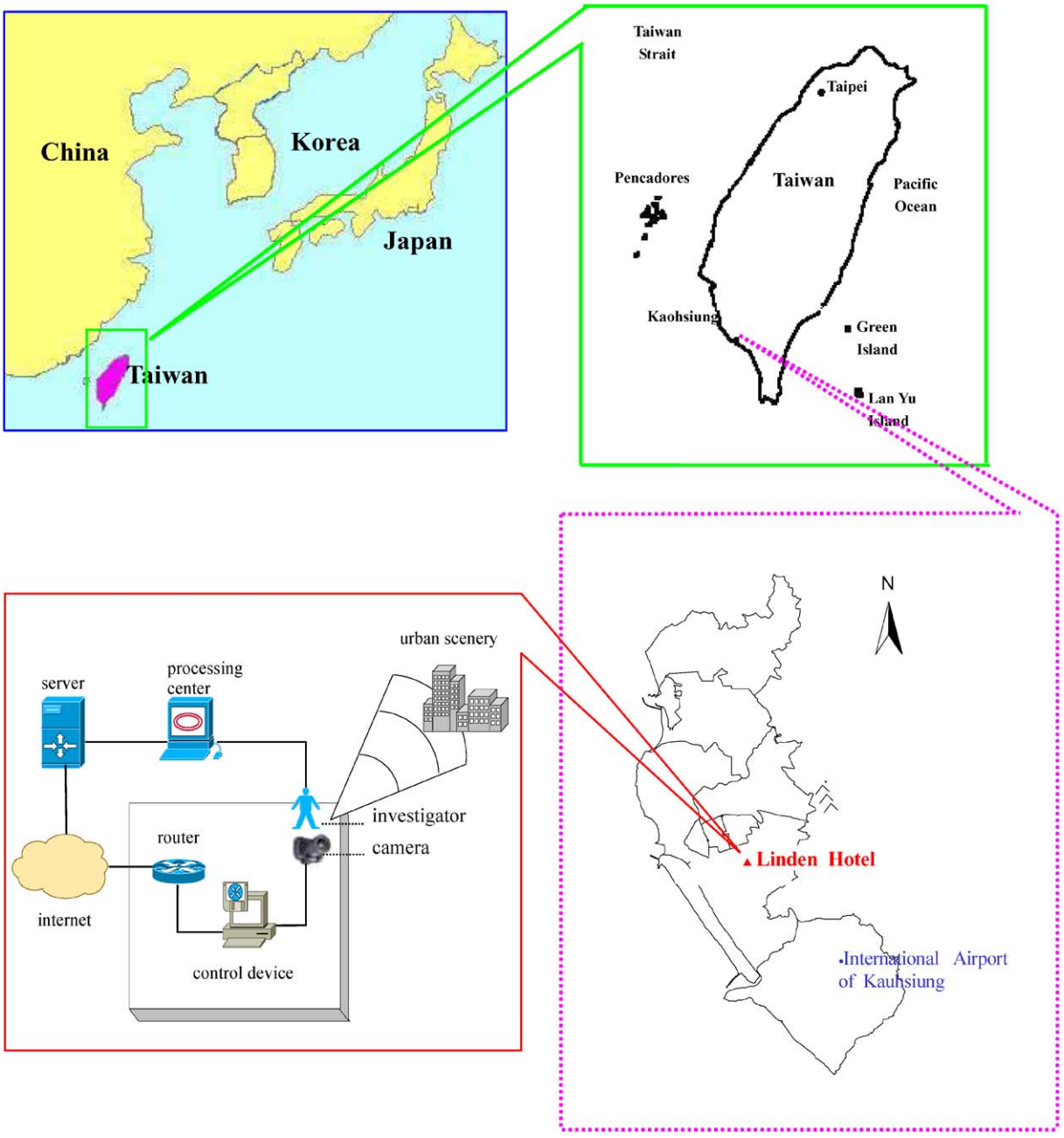

Fig. 3. Urban atmospheric image sampling and visual investigation on the top of Linden Hotel located at center of Kaohsiung, the southern city of Taiwan. Icons for computing and data transmission are from Cisco Products.

passed a test given by an expert at the Kaohsiung weather station. For image acquisition, urban atmospheric pictures were automatically taken by a digital camera (Kodak C 120) located in shadow to eliminate potential effects of sunlight. This camera equipped with triple-focus lens and charge-couple device (CCD) can generate a picture quality of 640×480 pixels. To simulate the photopic perception of far-gazing human eyes, camera focus was set to infinity (∞), and the camera's flash was not applied. Image sampling was performed twice between 10:40 a.m. and 14:20 p.m daily, from 1 January to 30 June, 2003. Before monitoring, the response of the CCD was checked with a standard multicolor chart (a digital image file). In enclosed

environment, the camera took a picture of the standard chart lit by an electric bulb with a color temperature of 5000 K. A digital comparison of the photograph of the chart and the chart itself confirmed the constancy of CCD quality. Finally, the high-frequency components in the digital images were extracted and two indices were sequentially estimated.

3.2. Field measurements

Table 1 illustrates the effects of extracting high-frequency components for the Sobel mask and FFT ($C_R = 10$ pixels) on two sampled images with large differences of visual range (12 vs. 3 km, i.e., good vs. poor visibility). For the clear image presenting good atmospheric visibility, the index values derived from the Sobel and FFT are 38.77 and 13.72. In comparison, the Sobel and FFT index values are 10.35 and 4.30, respectively, for the fuzzy image presenting poor visibility. More high-frequency components were extracted from the clear image than from the fuzzy image. Similar to the model illustrated in Fig. 1, larger values for the indices appeared for better atmospheric visibility.

The size of C_R for the FFT method was an important factor to control the pass ratio of high-frequency components in the image. Fig. 4 shows the C_R effect on the FFT index values for two images in Table 1 when C_R size was set to 0–200 pixels. When C_R size was larger than 2 pixels, a sharp cut of low-frequency components in the image occurred. When the value of C_R was larger than 100 pixels, the difference between clear and fuzzy images was not discernable because high-frequency components were almost ridded with the FFT filter. Therefore, a recommended range of C_R for FFT extraction was determined to be 5–30 pixels for expressing the high-frequency characteristics in an image.

Finally, relationships between observed visual range and two indices processed by the Sobel mask and FFT filter are shown in Fig. 5. The correlation coefficients (R^2) were 0.8139 and 0.7797 for the results obtained by

Table 1
Two urban atmospheric images and their high-frequency components extracted by Sobel mask and FFT ($C_R = 10$ pixels), respectively

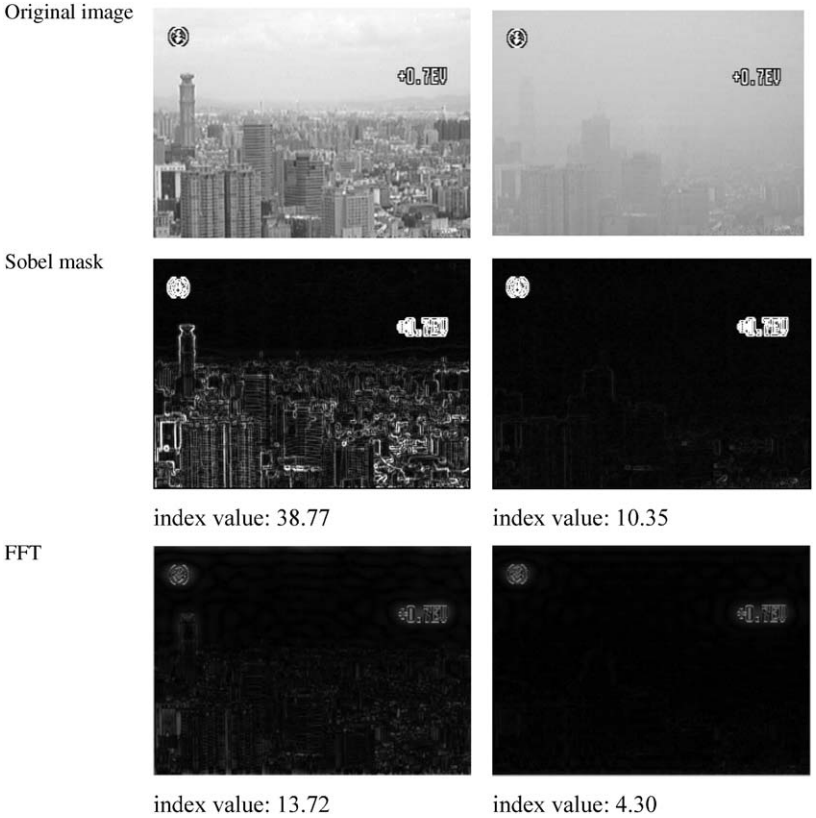

Left image (11:00, 4 May 2003): visual range 12 km (good visibility); right image (00:30, 20 May 2003): visual range 3 km (poor visibility).

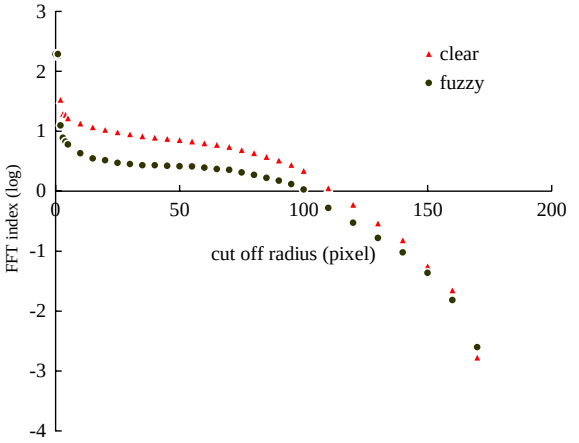

Fig. 4. The cut-off radius effect on the FFT index for both of clear and fuzzy images.

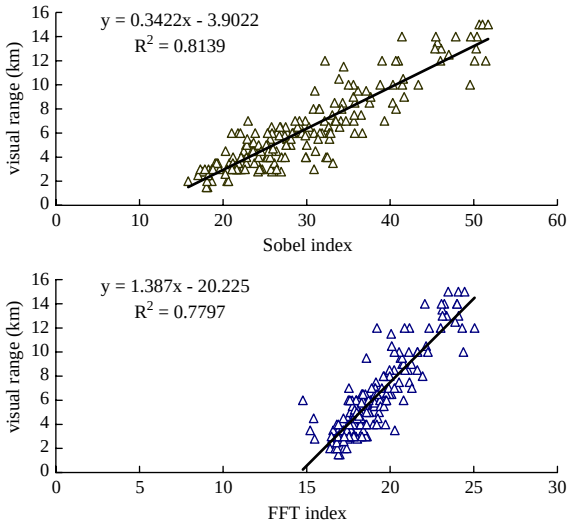

Fig. 5. Relationships between Sobel index (up), FFT index (down) and visual range measurements for the investigators, from 1 January to 30 June 2003.

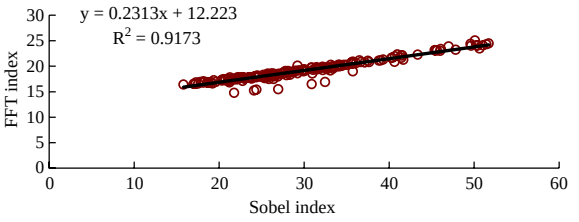

Fig. 6. Correlation between Sobel and FFT indices for sampled images.

the Sobel mask and FFT operation, respectively. In Fig. 6, there was good correspondence ($R^2 = 0.9173$) between Sobel and FFT indices for every sampled image. Therefore, it was confirmed that either of two extraction methods was a powerful tool for presenting urban atmospheric visibility by effectively extracting high-frequency information from the images.

4. Conclusions

Two image extraction methods were applied to isolate high-frequency information in the urban atmospheric images in an effort to improve visibility observation methods. Several novel approaches proved successful in this study. First, a model was developed to establish the relationship between high-frequency components in an image and urban visibility. Significant disturbance in an environmental image signal represented large visual range and good visibility of atmosphere. Second, digital data in urban images were effectively calculated by applying two image extraction methods: Sobel mask and FFT filter. Two independent indices were used to quantify high-frequency components merged in the atmospheric image. Third, experimental results predict that a perfect target is not necessary for visibility measurements in metropolitan areas because high-frequency information depends entirely on the brightness and texture in urban images. Furthermore, there was a good linear correlation between the values of the two indices and visual range estimated by the trained investigators. It was confirmed that the camera–computer system equipped with frequency extraction processing programs has the potential to record a visibility investigation in real-time. Consequently, sensitive areas in which visual perception is prized, such as airports, scenic spots, national parks, etc., can establish real-time images and monitor visibility by remote control through the methods proposed in this study.

Acknowledgements

The authors would like to thank the National Science Council of Taiwan for financially supporting this research under Contract No. NSC 93-2211-E-241-002.

References

Babson, B.L., Bergstrom, R.W., Samuelson, M.A., Seigneur, C., Waggoner, A., Malm, W.C., 1982. Statistical analysis of nephelometer regional field data. Atmospheric Environment 16, 2335–2346.

Dzubay, T.E., Steven, R.K., Lewis, C.W., Hern, D.H., Courtney, W.J., Tesch, J.W., Mason, M.A., 1982. Visibility and aerosol composition in Houston, Texas. Environmental Science and Technology 16, 514–525.

Gonzalez, R.C., Woods, R.E., 2002. Digital Image Processing, second ed. Pearson Education, Inc. publishing as Prentice-Hall, Englewood Cliffs, NJ.

Horvath, H., 1981. Atmospheric visibility. Atmospheric Environment 15, 1785–1796.

Larson, S.M., Cass, G.R., Hussey, K.J., Luce, F., 1988. Verification of image processing based visibility models. Environmental Science and Technology 22, 629–637.

Luo, C.H., Liu, S.H., Yuan, C.S., 2002. Investigate atmospheric visibility by the digital telephotography. Aerosol and Air Quality Research 2, 23–29.

Malm, W.C., Molenar, J.V., 1984. Visibility measurements in National Parks in the western United States. Journal of the Air Pollution Control Association 34, 899–904.

Middleton, W.E.K., 1963. Vision Through the Atmosphere. University of Toronto Press, Toronto.

Petrou, M., Bosdogianni, P., 1999. Image Processing: the Fundamentals. Wiley, England.

Pitchford, M.L., Malm, W.C., 1994. Development and applications of a standard visual index. Atmospheric Environment 28, 1049–1054.

Sequeira, R., Lai, K.H., 1998. The effect of meteorological parameters and aerosol constituents on visibility in urban Hong Kong. Atmospheric Environment 32, 2865–2877.

Tsai, Y.I., Cheng, M.T., 1997. Relationship between visibility, meteorological factors, and aerosol composition in the Taichung near-shore area. International Conference on Aerosol Technology/Environmental Measurement and Control Proceedings, pp. 76–84

Watson, J.G., 2002. Visibility, science and regulation. Journal of the Air and Waste Management Association 52, 628–713.

Williams, M., Chan, L.Y., Lewis, R., 1981. Validation and sensitivity of a simulated-photograph technique for visibility modeling. Atmospheric Environment 15, 2151–2170.

Yuan, C.S., Yang, H.Y., 1997. A study on the relationship of visibility with suspended particles and meteorological factors in Kaohsiung metropolitan area. International Conference on Aerosol Technology/Environmental Measurement and Control Proceedings, pp. 334–354.